Journal of Materials Chemistry A

Accepted Manuscript

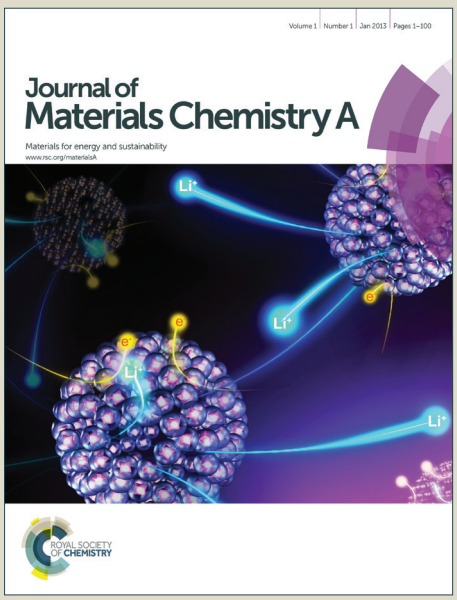

ROYAL SOCIETY OF CHEMISTRY

www.rsc.org/materialsA

Journal Name
Journal of Materials Chemistry A
Dynamic Article Links►

Cite this: DOI: 10.1039/c0xx00000x

www.rsc.org/xxxxxx

ARTICLE TYPE

A high performance cathode for proton conducting solid oxide fuel cells

Zhiquan Wang[a], Wenqiang Yang[a], Shahid P. Shafi[b], Lei Bi[b], Zhenbin Wang[a], Ranran Peng*[a,c,d], Changrong Xia[a], Wei Liu[a], Yalin Lu*[a,c,d]

Received (in XXX, XXX) XthXXXXXXXXX 20XX, Accepted Xth XXXXXXXXX 20XX
DOI: 10.1039/b000000x

Intermediate temperature solid-oxide fuel cells (IT-SOFC) has been becoming a worldwide need for reaching greater fuel efficiency, lower air pollution, much reduced cost and excellent longtime stability in energy conversion devices. In the intermediate temperature range (500-700°C), SOFCs based on proton conducting electrolytes (P-SOFCs) display unique advantages over those based on oxygen ion conducting electrolytes. A key obstacle to the practical operation of past P-SOFCs is the poor stability of the used traditional composite cathode materials in the steam-containing atmosphere and their low contribution to proton conduction. Here we report the identification of a new Ruddlesden Popper-type oxide $Sr_3Fe_2O_{7-\delta}$ that meets the requirements for much improved long-term stability and shows a superior single-cell performance. With a $Sr_3Fe_2O_{7-\delta}$-5wt.% $BaZr_{0.3}Ce_{0.5}Y_{0.2}O_{3-\delta}$ cathode in a uniform other than the common composite structure, the P-SOFC exhibits high power densities (683 and 583 Wcm^{-2} at 700 °C and 650 °C, respectively) when operated with humidified hydrogen as the fuel and air as the cathode gas. More importantly, no decay in discharging was observed within a 100-hour test.

1. Introduction

Demand for clean and renewable energy has aroused worldwide interests in intermediate-temperature solid-oxide fuel cells (IT-SOFCs) because of their great potential with long-term stability, economic competitiveness and conversion efficiency when in practical usage. Compared with IT-SOFCs using oxygen ion conductors (e.g., doped ceria), SOFCs with proton conductors (e.g. $BaCe_{0.8}Sm_{0.2}O_{2.9}$, $BaZr_{0.3}Ce_{0.5}Sm_{0.2}O_{2.9}$) in general can offer quite a few advantages[1-7]. Firstly, activation energy of proton transporting can be much lower than that for oxygen ion transporting, which may potentially offer a higher ionic conductivity at the intermediate temperature. Secondly, water product will be formed inside the cathode chamber, which will facilitate better fuel utilization efficiency and lower fuel cycling cost. Major progresses on proton conducting SOFCs (P-SOFCs) have been achieved, and single cells with acceptable power outputs have been reported by several research groups in the past.[1, 8-16] Nevertheless, it is still vital for P-SOFCs in regard of the unavailability of stable and highly conductive electrolytes, and also stable and efficient cathode materials.

Cathode electrochemical reactions for a P-SOFC are different with those for an oxygen ion conducting SOFC[17] (O-SOFC), as shown in equations 1 and 2, respectively. In an O-SOFC, the primary function of the cathode material is to facilitate the oxygen reductive dissociation and to accelerate the migration of formed oxygen ions to the electrolyte. In order to gain at this end, materials with good oxygen ionic and electronic mixed conductivities and with sufficient catalytic activities toward the oxygen reduction, for examples, $La_{0.6}Sr_{0.4}Co_{1-x}Fe_xO_{3-\delta}$ (LSCF), $Sm_{0.5}Sr_{0.5}CoO_{3-\delta}$ (SSC), $Ba_{0.5}Sr_{0.5}Co_{0.8}Fe_{0.2}O_{3-\delta}$ (BSCF), La_2NiO_4, are highly recommended. For a P-SOFC, however, protons transferred from electrolytes will react with oxygen to generate water molecule to be further released to gas phase. As depicted in equation 2, proton conduction, instead of oxygen ion conduction, should be vital to speed up the cathode reactions for a P-SOFC[6]. However, most cathode materials for P-SOFCs till now are those oxygen ion-electronic mixed conductors inherited from the O-SOFC. Therefore, the proton conducting phase (usually 30-60 wt.%) has to be added to form the composite structure in order to provide the proton transferring paths[7]. Typical materials include, for example, SSC-BZCY[18], LSCF-BZCY[12] and LSCF-BZPY[11]. Such traditional composite structured cathode materials, however, are unstable in the high water-containing atmosphere[19, 20]and are harmful to the long-term stability in a P-SOFC. Furthermore, effective reaction regions in these composite structured cathodes are highly restricted to the triple phase boundaries (proton/electronic/gas) and therefore will retard the cathodic reaction, as shown in Fig.1 (a).

However, if a uniform (single phase, other than the before mentioned composites) proton–electronic mixed conducting cathode being applied, the cathodic reaction area would be extended to the entire surface, and much improved cathodic reaction can be expected, as shown in Fig.1(b).

O-SOFC: $O_2+4e^-\rightarrow 2\,O^{2-}$ (1)

P-SOFC: $4H^++O_2+4e^-\rightarrow 2H_2O$ (2)

Early efforts to develop uniform proton-electron mixed conductors mainly focused on substituting altervalent elements into the proton conductors, such as $BaCe_{0.5}Bi_{0.5}O_{3-\delta}$[21], $BaCe_{0.85}Fe_{0.15}O_{3-\delta}$[22], $BaZr_{1-x}Pr_xO_{3-\delta}$[23], $BaCe_{0.4}Pr_{0.4}Y_{0.2}O_{3-\delta}$[1] and

Co-doped $BaZrO_3$[24]. Unfortunately, such past attempts are not so successful. Tao et al. demonstrated a $BaCe_{0.85}Fe_{0.15}O_{3-\delta}$ cathode based single cell[22], and the maximum power density was about 150 mW cm^{-2} at 700°C with a polarization resistance (Rp) of ~ 1.74 Ω cm^2. With a $BaCe_{0.4}Pr_{0.4}Y_{0.2}O_{3-\delta}$ single phase cathode, a polarization resistance of ~0.70 Ω cm^2 at 600 °C was achieved by Liu's group[1]. Rao et al used a $BaZr_{0.6}Co_{0.4}O_{3-\delta}$ cathode, and the polarization resistance was ~0.19 Ω cm^2.[24] Low performances of such uniform proton-electron mixed conducting cathodes mainly roots in their poor electronic conductivity. For example, electronic conductivities of $BaZr_{0.6}Co_{0.4}O_{3-\delta}$[24] and $BaZr_{0.4}Pr_{0.4}Y_{0.2}O_{3-\delta}$[25] are about 5.24 and 0.045 Scm^{-1}, respectively, at 700 °C[24], about 2 or 3 orders of the magnitude lower than those of typical cathode materials. Increasing the altervalent dopants' concentration is certainly helpful to improve the electronic conductivity; however, impurities might also form as the secondary phases.[22, 24, 26]

Ruddlesden-Popper (R-P) oxides with a general formula of $A_{n+1}B_nO_{3n+1}$, e.g. La_2NiO_4 and Pr_2NiO_4, have attracted wide attentions potentially as effective electrode materials. With their unique crystal structure where perovskite layers (n-ABO_3) sandwiched between rock-salt layers (AO), both high oxygen ion conductivity and electronic conductivity can be obtained in these oxides.[27, 28]Recently, high water-intercalation along with possible proton defects was detected in double layered R-P oxides $Sr_3Fe_2O_{7-\delta}$[29]. With the potential being a potential uniform proton-electronic mixed conductor, in this work, $Sr_3Fe_2O_{7-\delta}$ was firstly developed as a single-phase cathode for the P-SOFC. Effective proton concentration and conduction in the moist atmosphere have been suggested for $Sr_3Fe_2O_{7-\delta}$ by the density functional theory calculation, which enables it an interesting uniform and single phase cathode for P-SOFCs. With the new $Sr_3Fe_2O_{7-\delta}$ cathode, single cells based on $BaZr_{0.3}Ce_{0.5}Y_{0.2}O_{3-\delta}$ (BZCY) electrolytes demonstrate a good electrochemical performance with high peak power density of 683 $Wcm^{-2}$and a low polarization resistance of 0.07 Ωcm^{-2}at 700°C, among the best values ever reported so far. Importantly, our cells demonstrate so far the best long-term stability, to the best of our knowledge. Within the 100 hours' test, no performance degradation was observed when discharging at 0.2 Acm^{-2} at 700 °C.

2. Experimental

2.1 Preparation and Characterization of $Sr_3Fe_2O_{7-\delta}$ samples

$Sr_3Fe_2O_{7-\delta}$ (SFO) powders were synthesized using a solid-state reaction method. Stoichiometric amounts of $SrCO_3$ (99.9%, Sinopharm) and Fe_2O_3 (99.9%, Sinopharm) were mixed in ethanol and then ball milled for 48 hours. After drying at 90 °C for 6 hrs, the mixture was calcined at 1100 °C for 2 hrs to get the final powders. X-ray diffraction (XRD) analysis was performed to investigate the crystalline structure of the SFO powders using a Philips X'pert PRO diffract meter with Cu-Kα radiation at room temperature. Lattice parameters were fitted using FullProf 2011Rietveld refinement software.

$BaZr_{0.3}Ce_{0.5}Y_{0.2}O_{3-\delta}$ (BZCY)[30] and NiO[31] powders were prepared through combustion synthesis procedure, as reported previously. $Sr_3Fe_2O_{7-\delta}$ and BZCY mixture (1:1 in weight ratio) were co-fired at 1000 °C to investigate their chemical compatibility.

2.2Fabrication and testing of symmetric and single cells

For the fabrication of symmetric cells, BZCY powders were cold-pressed into disks of about 15 mm in diameter and 1 mm in thickness at 200 MPa, and then sintered at 1400 °C for 5 hrs to obtain dense electrolyte substrates. SFO (95wt.%) and BZCY (5wt.%) powders were mixed with ethocel and abietyl alcohol at a proper weight ratio to prepare the print-ink. The SFO electrodes with approximately 20 μm in thickness were formed by screen-printing the ink onto each side of the electrolyte substrate. The samples were fired at 1000 °C for 2hrs in air to form the symmetric cells. Ag paste was applied onto the electrode surface as the current collector.

Symmetric cells were tested from 500 to 700°C with a home-developed cell- testing system by A.C. impedance method using an electrochemical workstation (IM6e, Zahner). Measurements were conducted with the oxygen partial pressure ranging from 0.01 to 0.21 atm by using oxygen sensor (GNL-2100) with the general atmosphere pressure controlled at 1.00atm. The water vapor partial pressure of 0.05to 0.25 atm was achieved by heating the bubble at different temperatures. The frequency range applied for impedance measurements was from 0.01Hz to 1MHz. Curve fittings were performed using the Zview software.

For single cells fabrication, half cells of anode-supported thin electrolyte film were prepared by a co-pressing method using NiO-BZCY mixture as composite anode and BZCY as electrolyte, as described previously[30]. $Sr_3Fe_2O_{7-\delta}$ and BZCY mixtures in the weight ratio of 95:5 were blended with a 6wt.% ethylcellulose – terpineol binder to obtain the cathode slurry. The slurry was screen-printed on the surface of electrolyte films, and then sintered at 1000°C for 2 h in air to complete the fabrication of single cells.

Single cells were tested in a home-developed cell-testing system using humidified hydrogen (~3% H_2O) as the fuel and the atmospheric air as oxidant. The flow rate of the fuel gas was about 20 ml min^{-1}. A.C. impedance spectra and the discharging properties of the cells were investigated using an electrochemistry workstation (IM6e, Zahner). Fracture microstructures of the cells after testing were analyzed using a JEOL scanning electron microscopy (SEM, JXA-8100).

2.3 Computational details

First-principles calculation method was adopted to study the bulk proton formation and migration energies. All total energy calculations were based on the projector augmented wave (PAW) [32]method, implemented in Vienna ab initio simulation package (VASP) [33, 34]. The Perdew-Burke-Ernzerh of (PBE) [35] functional was used to treat the exchange-correlation effects. The kinetic energy cutoff was set to 450 eV and the energy convergence criterion was 10^{-5} eV per unit cell. In the structure optimization performance, the Hellmann-Feynman force on each atom was smaller than 0.01 $eVÅ^{-1}$. Ferromagnetic (FM) states were applied in order to simplify the calculations. And all calculations were spin-polarized. DFT+U[36] theory is used with U_{eff} = 5.3 eV applied to Fe ions.

3. Results and discussion

3.1 Properties of SFO samples

Fig.2 shows the Rietveld fit of the X-ray diffraction (XRD) pattern of $Sr_3Fe_2O_{7-\delta}$ (SFO) powders carried out using FullProf 2011 program. The peaks can be indexed on a tetragonal unit cell with space group I4/mmm. The background was fitted using a cubic spline during the initial stage of the refinement and fixed for the subsequent refinement cycles. A total of 12 parameters including unit cell parameters, scale factor, peak shape parameters, atomic positions and zero point were refined. The reliability factors obtained were Rp = 3.70, Rwp = 5.27, $\chi 2$ = 5.31. The tetragonal phase structural parameters obtained based on this model are a = b = 3.86683(6) Å, c = 20.1737(4) Å, in good accordance with the values in PDF#820416[26]. Fig.3 shows the crystal structure of $Sr_3Fe_2O_{7-\delta}$ according to the Rietveld analysis result. Good chemical compatibility between SFO and BZCY mixture co-fired at 1000 °C, the cathode fabrication temperature, can be also observed. As shown in Fig. 4, no impurities formed at this heating temperature.

As depicted in supporting information Fig. S1 and S2, $Sr_3Fe_2O_{7-\delta}$ is a good oxygen ion-electronic conductor with high surface exchange coefficient in dry atmosphere. Yet, with respect to its proton conduction in moist atmosphere, we failed to get direct access to the values using hydrogen permeation method because of the low chemical stability of $Sr_3Fe_2O_{7-\delta}$ in reducing condition. Here, we used the first-principle calculation based on DFT (Density Functional Theory) method to reveal the possible proton conducting property in $Sr_3Fe_2O_{7-\delta}$. The calculations were carried out on a 2x2x1 96 atoms I4/mmm super cells of $Sr_3Fe_2O_{7-\delta}$with a 3x3x1 Monkhorst-Packk-point mesh for the integration over the first Brillouin zone. Proton defects ($OH_O^{\bullet}$) might form at three different oxygen atoms, depicted in Fig. 3 as d1, d2 and d3, and the corresponding proton formation energies at d1, d2 and d3 sites are -0.23, -0.34 and -1.44 eV, respectively, suggesting that protons prefer to form at d3 sites. It should be noted that the calculated values of formation energies for proton defects are all negative here, indicating that the formed proton defects are energetically stable in the $Sr_3Fe_2O_{7-\delta}$.

Two representative proton diffusion pathways were mapped out to examine the proton mobility in the SFO cathode. Fig. 5 (a) and (b) illustrate the proton migrating processes along [001] and [010] directions via rotation (R) and transfer (T) approach, respectively. An overall proton migration pathway along the [001] direction can be summarized as the following process: T12 → R23 → R34 → T45 → T56 (forward) and T65 →T54 →R43 → R32 → R21 (backward, or the intensive forward in next periodic block). The migration barriers of proton involving in these processes are summarized in Table 1. We found that T56 and T65 processes (proton transferring from one SrO layer to the adjacent SrO layer) offer the highest migration barrier of 0.62 eV and T45 process has the lowest migration barrier of 0.00 eV. This result indicates that the protons formed at d3 (SrO) prefer to transfer to the perovskite layer rather than to another SrO layer. We attribute this noticeable difference to the special trapping effect of the SrO layer to proton transferring. And therefore, the process of proton transferring away from SrO layer suffers from the trapping effect (T56, T65 and T54) whereas that proton diffusing to a SrO layer (T45) benefits from the special attraction. This is also consistent with the calculation results of proton formation energies, where d3 (in SrO layer) has the lowest formation energy values. It should be also noted that T45 and T54 also propose a transferring path for protons along [010] direction within the SrO layer.

To map out the proton transferring paths along [001] direction, we adopted those within the perovskite slab since those along SrO layer has been proposed by the above calculation. Fig. 5b shows the migrating process for protons via T12 → T23 → R34 → R45 (41) along the [010] direction. The migration energies for those pathways are summarized in Table 2, and T12 gives the highest migration energy barrier of 0.28 eV. Along the [010] direction, the highest migration energy barrier of proton is about 0.34 eV lower than that along the [001] direction. Yet, considering the relatively small proton formation energies at d1 and d2 sites and the large energy barrier for protons transferring SrO layer to perovskite slab (T54), we cannot conclude that the proton diffusing within perovskites ([010] direction) is more dominant than that through SrO layer ([001] direction). It should be also noted that the proton transporting along other directions can all be considered as the combination of the elementary steps along [001] and [010] directions.

Remarkably, the energy barrier for proton diffusion in SFO is within the typical range for $BaZrO_3$ doped with Y [37, 38], and Co[39] as dopants. The low energy barrier for proton migration and the low proton formation energy strongly suggest very good proton conduction in SFO in humid atmosphere and enable SFO as a promising cathode for P-SOFC along with its sufficient electronic conductivity.

3.2 Characterizations of single cells

Single cells with SFO based cathodes were characterized using wet H_2 as fuel and static air as oxidant. To improve the contact between electrolyte and $Sr_3Fe_2O_{7-\delta}$cathode, 5wt.% BZCY is added in $Sr_3Fe_2O_{7-\delta}$ cathode. The SEM image of the tested cell using SFO-BZCY (5wt%) cathode is shown in Fig.S6. The electrolyte is very dense and adheres well to both electrodes. The thickness of the electrolyte and cathode are 14 and 20 μm, respectively.

Discharging performance of the cells with $Sr_3Fe_2O_{7-\delta}$ cathode is presented in Fig. 6(a), of which maximum power densities with the values of 683, 530 and 372 $mWcm^{-2}$ are achieved at 700, 650 and 600 °C, respectively. With $Sr_3Fe_2O_{7-\delta}$ cathode, the cells offer better electro-performance than those using composite cathodes, for examples, SSC-$Ce_{0.8}Sm_{0.2}O_{1.9}$ (SDC) (504 $mWcm^{-2}$ at 650 °C)[10], SSC-$BaZr_{0.3}Ce_{0.5}Y_{0.16}Zn_{0.04}O_{3-\delta}$ (BZCYZ) (364 $mWcm^{-2}$ at 650 °C)[40], $PrBaCo_2O_{5+\delta}$-BZCYZ (266 $mWcm^{-2}$ at 650 °C)[41] , LSCF- $BaZr_{0.5}Pr_{0.3}Y_{0.2}O_{3-\delta}$ (BZPY30) (~130 $mWcm^{-2}$ at 650 °C)[11] composite cathodes.

EIS plots of the cells using $Sr_3Fe_2O_{7-\delta}$ cathode under open circuit conditions are shown in Fig. 6(b). The polarization resistances, determined from the arc length of the impedance spectra, reduce with the increasing testing temperatures, about 0.07, 0.15, and 0.35Ωcm^2 measured at 700, 650, and 600 °C, respectively. Comparisons in Rp values for cells with different cathodes are shown in Fig. 7. Among various cathode materials including both composite cathodes and single phase cathodes, $Sr_3Fe_2O_{7-\delta}$ cathode based cells offer the lowest Rp values [10, 12, 13,

[16, 21, 42], suggesting promising electro-catalysis and good ionic transporting properties of $Sr_3Fe_2O_{7-\delta}$ cathode. Especially, an increasing loss in the discharging performance of cells can be observed with the increase of BZCY weight ratio in $Sr_3Fe_2O_{7-\delta}$–BZCY cathodes, as shown in Fig.8. With the BZCY weight ratio of 15%, 25% and 35%, the maximum power densities of cells are 379, 313 and 175 $mWcm^{-2}$, respectively, measured at 650 °C. The depressed performance with higher BZCY content, resulting from the increase of the polarization resistance as shown in Fig.S4 (ESI†), strongly suggests the good proton conduction in SFO and the effectiveness of SFO single phase cathode if the adhesion problem not considered.

Remarkably, with SFO cathode, the cell presents the best long-term stability so far. As shown in Fig. 9, no performance degradation is observed within the 100 hours' test. While with SSC-BZCY (35wt.%) cathode, the cell fails completely after 12 hours' test. The good electrochemical performance and great long-term stability highly recommend SFO as an excellent cathode for P-SOFC.

3.3 Symmetric cells performance

Impedance spectra of the symmetrical cell using a $S_3Fe_2O_{7-\delta}$-5wt.%BZCY electrode were measured in various atmospheres to further investigate its cathodic electro-performance. As shown in Fig. 10(a) and (b), two depressed arcs are observed in each spectrum measured in humid atmosphere, a small high-frequency arc and a large low-frequency arc with relaxation frequencies of 6309 Hz and 0.5 Hz, respectively, implying two rate-limiting steps at least. An equivalent circuit composed of two RQ elements (R_HQ_H) (R_LQ_L) are proposed to resolve these spectra, as shown in Fig.S5 (ESI†), where R represents the polarization resistance, Q represents the constant phase element, and the subscripts H and L correspond to the high and low frequency arc, respectively. As shown in Fig. 10(c), both R_H and R_L reduce with the increase of oxygen partial pressures, while keeps almost constant with the increase of steam partial pressures, suggesting that these rate-limiting steps are not proton related reactions.

Typically, the dependence of R_H and R_L on oxygen partial pressure (P_{O_2}) and steam partial pressure (P_{H_2O}) can be presented in the usual form of

$$\log(1/Ri) \prec P_{O_2}^{n} P_{H_2O}^{m},$$

here n and m are deemed as reaction order of Ri with respect to P_{O_2} and P_{H_2O} , respectively. As shown in Fig. 10(c), the fitted n_H and n_L with respect to oxygen partial pressure are close to 1/4 (0.23±0.015) and 3/8 (0.34±0.033), respectively, and with respect to water partial pressure are almost zero. This result is quite different to those for $Sm_{0.5}Sr_{0.5}CoO_{3-\delta}$(SSC)-$BaCe_{0.8}Sm_{0.2}O_{3-\delta}$ (BCS)[43], of which R_H is independent to P_{O_2} whereas has a reaction order of 1/2 to P_{H_2O} , and R_L has a reaction order of 1/4 with respect to P_{O_2} where as independent to P_{H_2O} , suggesting different rate limiting steps[43]. The activity energies for the R_H and R_L can be fitted as 1.36 and 1.42 eV, respectively, as shown in Fig. 11.

The dependence of R_H and R_L of SFO cathode on P_{O_2} and P_{H_2O} , can be concluded as Eq. (1) and Eq. (2):

$$R_H \prec P_{O_2}^{1/4} P_{H_2O}^{0} \quad (1)$$

$$R_L \prec P_{O_2}^{3/8} P_{H_2O}^{0} \quad (2)$$

To confirm the rate limiting steps, detailed reaction processes for SFO cathode, a proton-electronic mixed conductor, are proposed, as illustrated in Fig. 12: 1) the surface adsorption and dissociation of oxygen molecules; 2) the reduction of oxygen atom to O^-; 3) the incorporation of O^- into $Sr_3Fe_2O_{7-\delta}$ lattice; 4)the reduction of O^- to O^{2-}; 5) protons migrating from electrolyte to the SFO surface; and 6-7) protons reacts with the incorporated oxygen species to form water molecule; and 8) desorption of H_2O from SFO into gas phase. Table.3 summarized the elementary steps and the calculated reaction orders of each step with respect to P_{O_2} and P_{H_2O} .

As shown in Table.3, step 2 and step 3 have similar dependence on P_{O_2} and P_{H_2O} with the R_L and R_H, respectively, suggesting that the reduction of adsorbed oxygen atom and the incorporation of O^- into lattice should be the rate-limiting steps for $Sr_3Fe_2O_{7-\delta}$ cathode. Unlike those of SSC-BCS cathode[43], proton related steps seem to be pretty quick for SFO cathode[11, 14]. The high activity energies for the R_H and R_L also support this much statement since they are much higher than that for proton conduction, usually 0.4-0.6eV.

4. Conclusions

The present study demonstrated that high power densities and stable power output could be achieved in IT-SOFCs based on proton conductors using a proper cathode $Sr_3Fe_2O_{7-\delta}$. The $Sr_3Fe_2O_{7-\delta}$ cathode with Ruddlesden-Popper structure offers unique ion (proton and/or oxygen ion)-electronic transporting properties, depending on the steam content in the testing atmosphere, and excellent surface exchange coefficient of oxygen, facilitating the cathodic electrochemical reactions in P-SOFCs. With $Sr_3Fe_2O_{7-\delta}$-5wt.%BZCY as cathode, a maximum power density of 683 $mWcm^{-2}$ was achieved at 700°C for a single cell. Furthermore, great discharging stability of the single cell with $Sr_3Fe_2O_{7-\delta}$ as cathode has been demonstrated through a 100 hours' test.

Acknowledgements

This work was financially supported by the Natural Science Foundation of China (51472228), the National Basic Research Program of China (973 Program, 2012CB922001 and 2012CB215403), and the Fundamental Research Funds for the Central Universities (WK2060190025). The authors acknowledge the Supercomputing Center of USTC for providing computational resources

Notes and references

[a]*CAS Key Laboratory of Materials for Energy Conversion, Department of Materials Science and Engineering, University of Science and Technology of China, Hefei, 230026 Anhui, China*
[b]*Physical Sciences and Engineering Division, King Abdullah University of Science and Technology (KAUST), Thuwal 23955-6900, Saudi Arabia*
[c]*Synergetic Innovation Center of Quantum Information & Quantum Physics, University of Science and Technology of China, Hefei, Anhui 230026, China*

[d]*Hefei National Laboratory of Physical Science at the Microscale, University of Science and Technology of China, Hefei, 230026 Anhui, China*
Email: pengrr@ustc.edu.cn ,Tel&Fax: ++86-551 63600594
Email: yllu@ustc.edu.cn ,Tel&Fax: ++86-551 63603004

† Electronic Supplementary Information (ESI) available:experimental details of conductivity, oxygen permeation and electrical conductivity relaxation tests; the results of electronic conductivity, oxygen permeation rate,surface exchange coefficients, BZCY content dependence of the ohmic resistance (Ro) and the polarization resistance (Rp), experimental and fit Nyquist plots. See DOI: 10.1039/b000000x/

1. C. Zuo, S. Zha, M. Liu, M. Hatano and M. Uchiyama, *Advancedmaterials*, 2006, 18, 3318-3320.
2. S. W. Tao and J. T. S. Irvine, *Advanced materials*, 2006, 18, 1581-1584.
3. R. Haugsrud and T. Norby, *Nature materials*, 2006, 5, 193-196.
4. K. D. Kreuer, *Annual Review of Materials Research*, 2003, 33, 333-359.
5. K.-D. Kreuer, S. J. Paddison, E. Spohr and M. Schuster, *Chemical reviews*, 2004, 104, 4637-4678.
6. E. Fabbri, L. Bi, D. Pergolesi and E. Traversa, *Advanced materials*, 2012, 24, 195-208.
7. E. Fabbri, D. Pergolesi and E. Traversa, *Chemical Society reviews*, 2010, 39, 4355-4369.
8. G. Taillades, J. Dailly, M. Taillades-Jacquin, F. Mauvy, A. Essouhmi, M. Marrony, C. Lalanne, S. Fourcade, D. J. Jones, J. C. Grenier and J. Rozière, *Fuel Cells*, 2010, 10, 166-173.
9. E. Fabbri, L. Bi, H. Tanaka, D. Pergolesi and E. Traversa, *Advanced Functional Materials*, 2011, 21, 158-166.
10. W. Sun, L. Yan, B. Lin, S. Zhang and W. Liu, *Journal of Power Sources*, 2010, 195, 3155-3158.
11. E. Fabbri, L. Bi, D. Pergolesi and E. Traversa, *Energy & Environmental Science*, 2011, 4, 4984.
12. L. Yang, Z. Liu, S. Wang, Y. Choi, C. Zuo and M. Liu, *Journal of Power Sources*, 2010, 195, 471-474.
13. J. Hou, Z. Zhu, J. Qian and W. Liu, *Journal of Power Sources*, 2014, 264, 67-75.
14. C. Zhang and H. Zhao, *Journal of Materials Chemistry*, 2012, 22, 18387.
15. Y. Lin, R. Ran, D. Chen and Z. Shao, *Journal of Power Sources*, 2010, 195, 4700-4703.
16. M. Shang, J. Tong and R. O'Hayre, *RSC Advances*, 2013, 3, 15769.
17. C. Sun, R. Hui, J. Roller, *J Solid State Electrochem*, 2010, 14, 1125-1144
18. L. Yang, C. Zuo, S. Wang, Z. Cheng and M. Liu, *Advanced materials*, 2008, 20, 3280-3283.
19. S. H. Kim, K. B. Shim, C. S. Kim, J. T. Chou, T. Oshima, Y. Shiratori, K. Ito and K. Sasaki, *Journal of Fuel Cell Science and Technology*, 2010, 7, 021011.
20. R. R. Liu, S. H. Kim, S. Taniguchi, T. Oshima, Y. Shiratori, K. Ito and K. Sasaki, *Journal of Power Sources*, 2011, 196, 7090-7096.
21. Z. Tao, L. Bi, L. Yan, W. Sun, Z. Zhu, R. Peng and W. Liu, *Electrochemistry Communications*, 2009, 11, 688-690.
22. Z. Tao, L. Bi, Z. Zhu and W. Liu, *Journal of Power Sources*, 2009, 194, 801-804.
23. E. Fabbri, I. Markus, L. Bi, D. Pergolesi and E. Traversa, *ECS Transactions*, 2011, 35, 2305-2311.
24. Y. Rao, S. Zhong, F. He, Z. Wang, R. Peng and Y. Lu, *International Journal of Hydrogen Energy*, 2012, 37, 12522-12527.
25. E. Fabbri, I. Markus, L. Bi, D. Pergolesi and E. Traversa, *Solid State Ionics*, 2011, 202, 30-35.
26. C. Zhang and H. Zhao, *Electrochemistry Communications*, 2011, 13, 1070-1073.
27. A. A. Markov, M. V. Patrakeev, V. V. Kharton, Y. V. Pivak, I. A. Leonidov and V. L. Kozhevnikov, *Chemical reviews*, 2007, 19, 3980-3987.
28. I. Kagomiya, K. Jimbo, K. Kakimoto, M. Nakayama and O. Masson, *Physical chemistry chemical physics : PCCP*, 2014, 16, 10875-10882.
29. M. Matvejeff, M. Lehtima, A. Hirasa, Y. H. Huang, H. Yamauchi and M. Karppinen, *Chemical reviews*, 2005, 17, 2775-2779.
30. Y. Rao, Z. Wang, W. Zhong, R. Peng and Y. Lu, *Journal of Power Sources*, 2012, 199, 142-145.
31. W. Zhu, C. Xia, J. Fan, R. Peng and G. Meng, *Journal of Power Sources*, 2006, 160, 897-902.
32. P. E. Blöchl, *Physical Review B*, 1994, 50, 17953-17979.
33. G. Kresse and J. Furthmuller, *Physical Review B*, 1996, 54, 169-186.
34. G. Kresse and J. Hafner, *Physical Review B*, 1993, 48, 13115-13118.
35. J. Perdew, K. Burke and M. Ernzerhof, *Physical Review Letters*, 1996, 77, 3865-3868.
36. S. Dudarev, G. Botton, S. Savrasov, C. Humphreys and A. Sutton, *Physical Review B*, 1998, 57, 1505-1509.
37. B. Merinov and W. Goddard, *The Journal of chemical physics*, 2009, 130, 194707.
38. S. J. Stokes and M. S. Islam, *Journal of Materials Chemistry*, 2010, 20, 6258.
39. Z. Wang, W. Yang, Z. Zhu, R. Peng, X. Wu, C. Xia and Y. Lu, *Journal of Materials Chemistry A*, 2014, 2, 16707-16714.
40. H. Ding, X. Xue, X. Liu and G. Meng, *Journal of Alloys and Compounds*, 2010, 494, 233-235.
41. M. Jin, X. Zhang, Y. e. Qiu and J. Sheng, *Journal of Alloys and Compounds*, 2010, 494, 359-361.
42. Y. Lin, W. Zhou, J. Sunarso, R. Ran, Z. Shao, *International Journal of Hydrogen Energy,* 2012, 37, 484-497.
43. F. He, T. Wu, R. Peng and C. Xia, *Journal of Power Sources*, 2009, 194, 263-268.

Cite this: DOI: 10.1039/c0xx00000x

www.rsc.org/xxxxxx

ARTICLE TYPE

Table.1. The bulk proton migration energy barriers along [001] direction in $Sr_3Fe_2O_7$

[001]	1→2	2→3	3→4	4→5	5→6
Forward/eV	0.25	0.32	0.25	0.00	0.62
Backward/eV	0.05	0.08	0.27	0.53	0.62

Table.2. The bulk proton migration energy barriers along [010] direction in $Sr_3Fe_2O_7$

[010]	1→2	2→3	3→4	4→5
Forward/eV	0.28	0.05	0.18	0.18

Table.3. Elementary cathode reaction steps and their reaction orders with respect to oxygen partial pressure (n) and water vapor partial pressure (m)

	Elementary reaction	n	m
Step 1	$O_{2(g)} \rightarrow 2O_{ad}$	1	0
Step2	$O_{ad} + e^- \rightarrow O_{ad}^-$	3/8	0
Step3	$O_{ad}^- \rightarrow O_{lattice}^-$	1/4	0
Step6	$O_{lattice}^- + e^- \rightarrow O_{lattice}^{2-}$	0	0
Step4	$H_{bulk}^+ \rightarrow H_{surface}^+$	0	1/2
Step5	$O_{lattice}^{2-} + H_{surface}^+ \rightarrow OH_{lattice}^-$	0	1/2
Step7	$OH_{lattice}^- + H_{surface}^+ \rightarrow H_2O_{ad}$	0	1
Step8	$H_2O_{(ad)} \rightarrow H_2O_{(g)}$	0	1

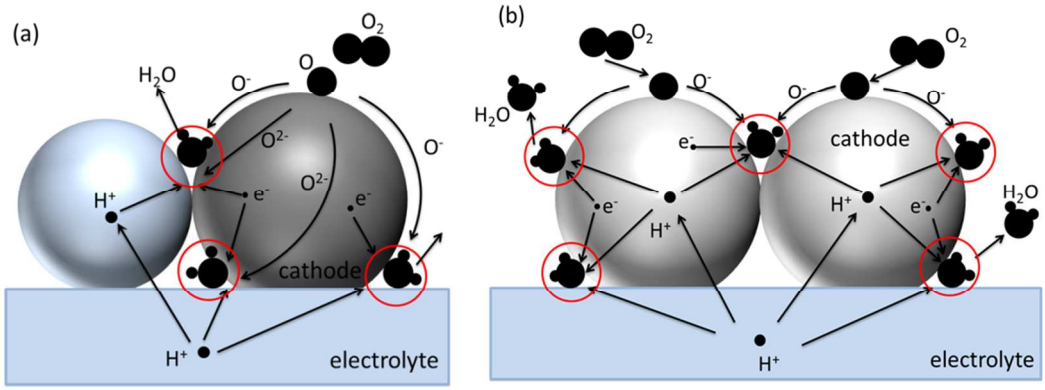

Fig.1 Schematic of the reaction at the cathode electrode for P-SOFCs using:(a) a composite cathode made of a proton-conducting oxide and an oxygen ion-electron mixed conducting oxide; (b) a proton and electron mixed conducting oxide.

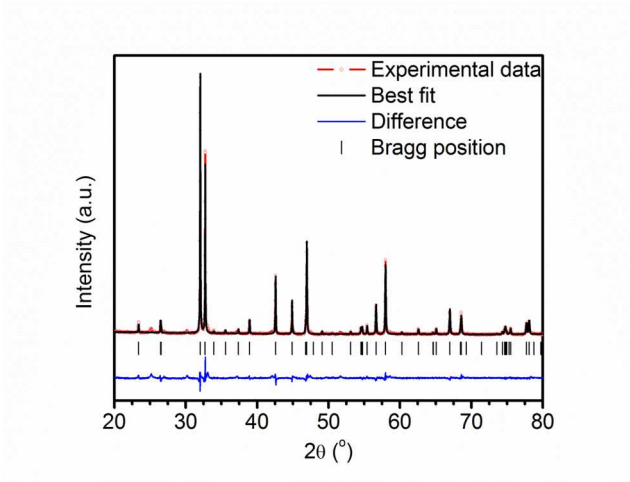

Fig.2. XRD Rietveld refinement of $Sr_3Fe_2O_{7-\delta}$ prepared by a solid state reaction method

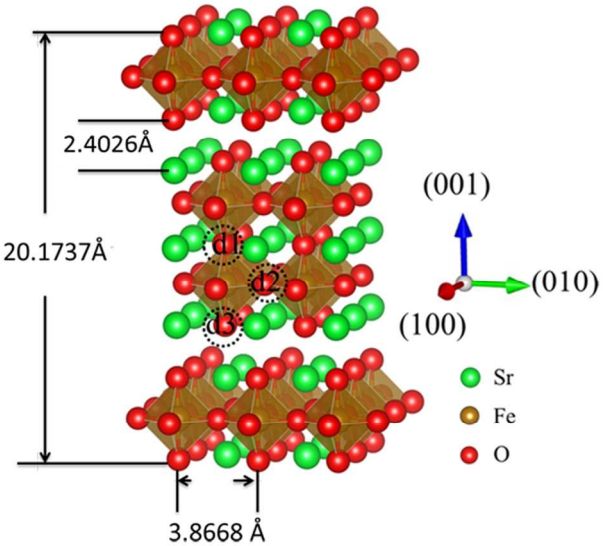

Fig.3. The crystal structure of $Sr_3Fe_2O_{7-\delta}$ oxide. Here, d1-d3 denote three types of oxygen sites for possible proton defects formation.

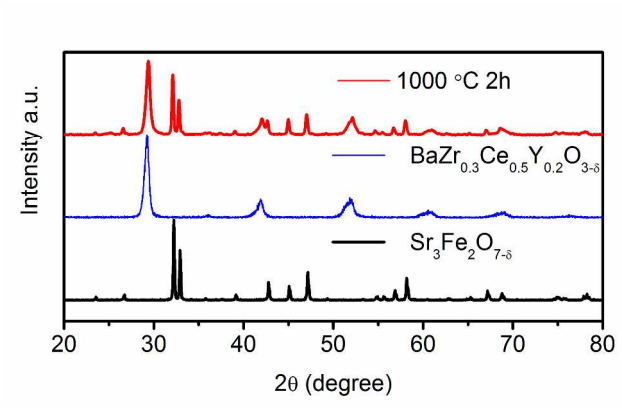

Fig.4. XRD patterns of $BaZr_{0.3}Ce_{0.5}Y_{0.2}O_{3-\delta}$(blue), $Sr_3Fe_2O_{7-\delta}$(black) and the $BaZr_{0.3}Ce_{0.5}Y_{0.2}O_{3-\delta}$-$Sr_3Fe_2O_{7-\delta}$ mixture(1:1 in weight ratio) co-fired at 1000 °C.

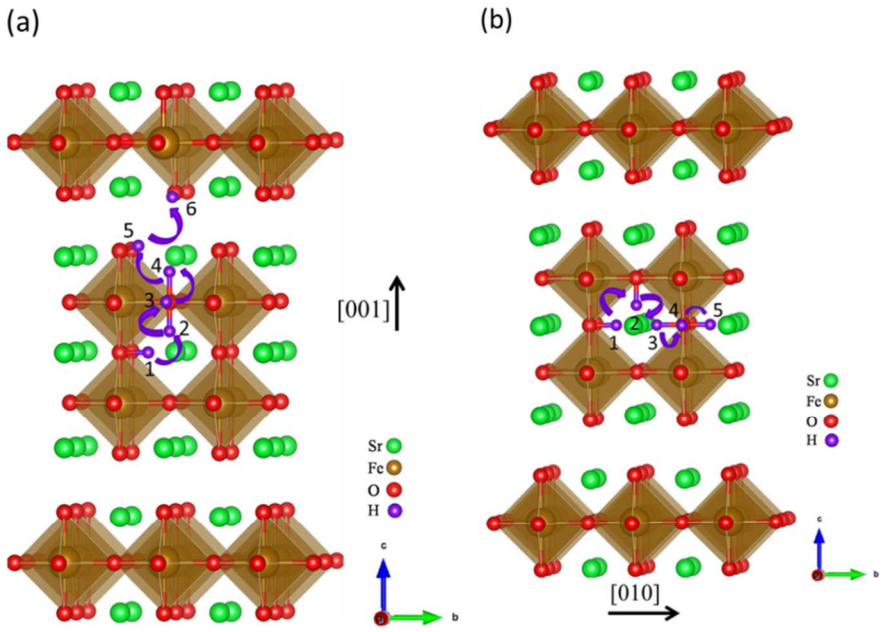

Fig.5 Schematic representations of the proton transporting along (a) [001] and (b)[010] directions

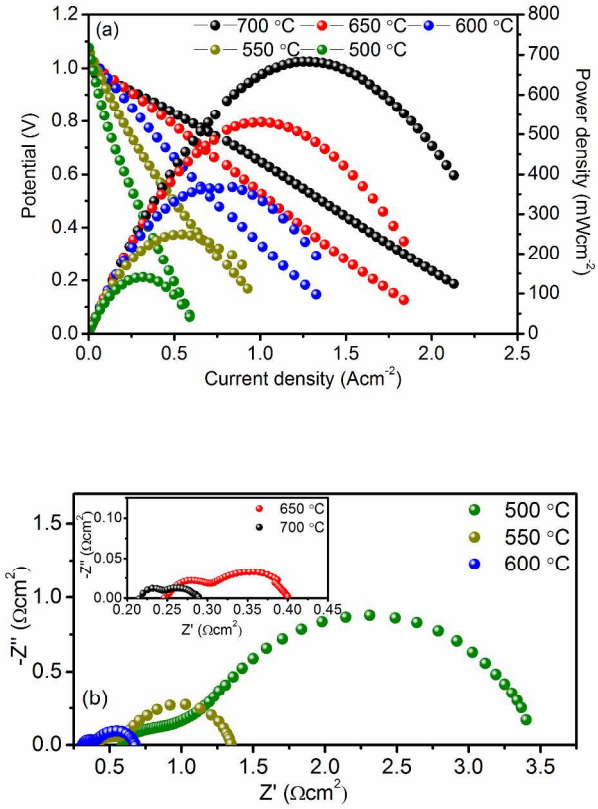

Fig.6. (a) the I-V curves and (b) the impedance spectra of the single cell with a $Sr_3Fe_2O_{7-\delta}$-5wt.% BZCYcathode measured at various temperatures.

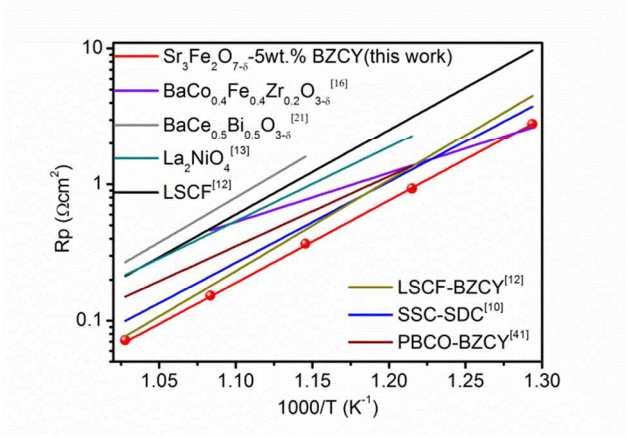

Fig.7. Comparison of the polarization resistance of $Sr_3Fe_2O_{7-\delta}$-5wt.% BZCY cathode with difference cathodes as determined from impedance spectra measured under open circuit conditions.

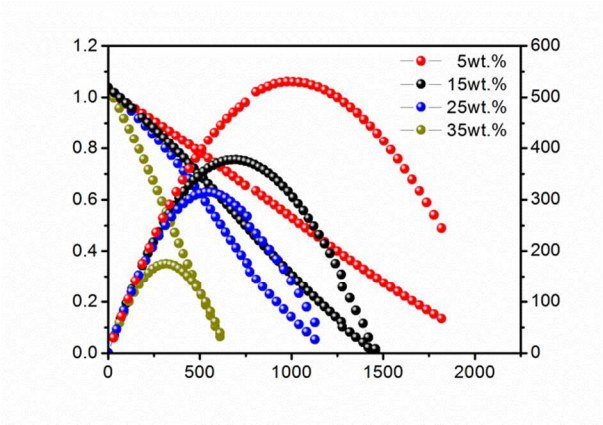

Fig.8 I-V and I-P curves of cells as function of BZCY weight ratio in SFO/BZCY composite cathodes measured at 650 °C.

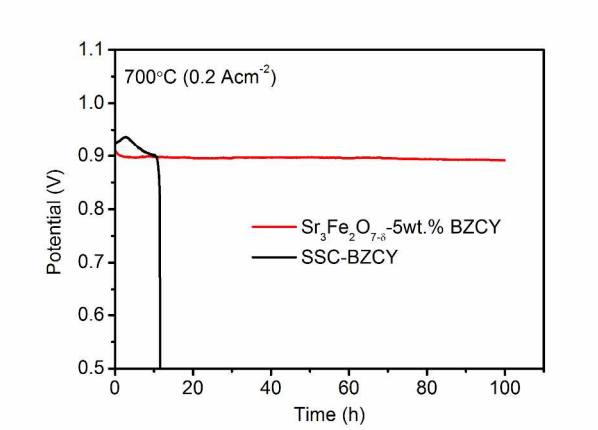

Fig.9. The long-term stability of $Sr_3Fe_2O_{7-\delta}$-5wt.%BZCY and SSC-BZCY cathodes at the discharging current density of 0.2 Acm^{-2} at 700 °C.

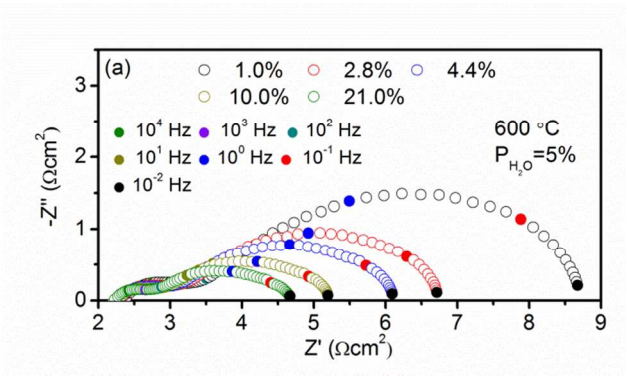

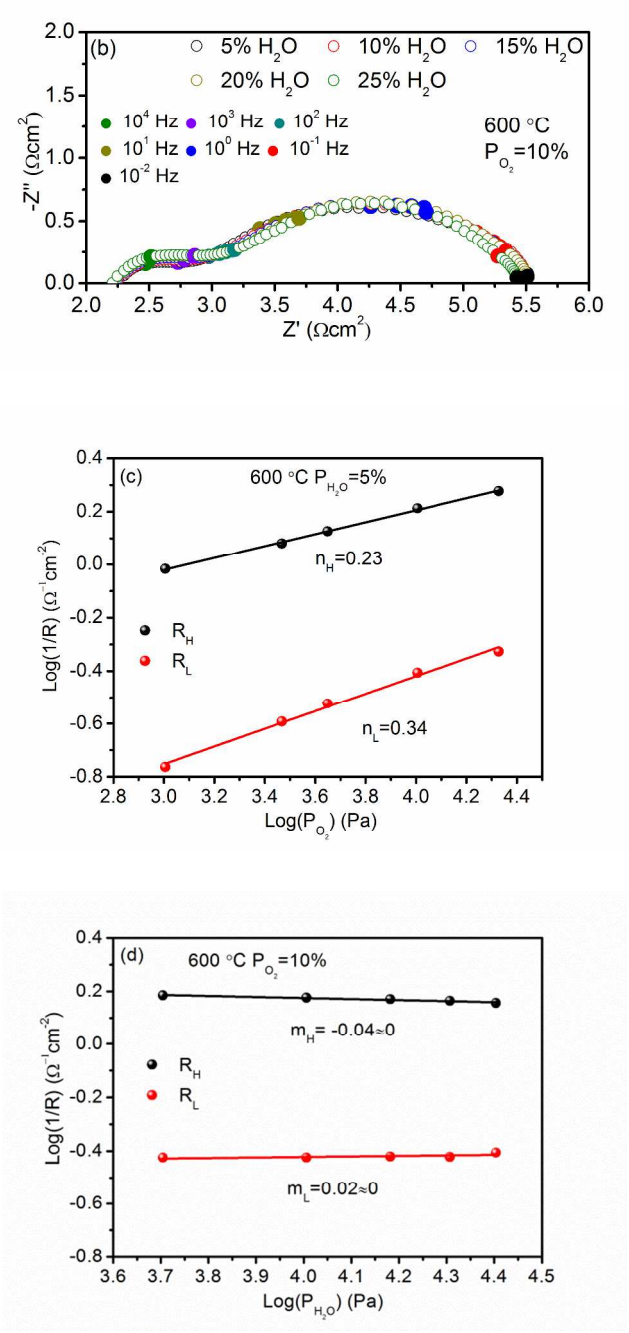

Fig.10. The impedance spectra of the symmetrical cells using $Sr_3Fe_2O_{7-\delta}$-5wt.%BZCYas cathode measured at 600 °C with (a) various oxygen partial pressures; and (b) various steam partial pressures; and (c) oxygen partialpressure (P_{O_2}) dependence of high-frequency resistance (R_H, black) and low-frequency resistance (R_L, red) measured in humidified N_2–O_2 atmospheres, respectively; and (d) steam partial pressure (P_{H_2O}) dependence of high-frequency resistance (R_H, black) and low-frequency resistance (R_L, red) measured in humidified N_2–O_2 atmospheres, respectively

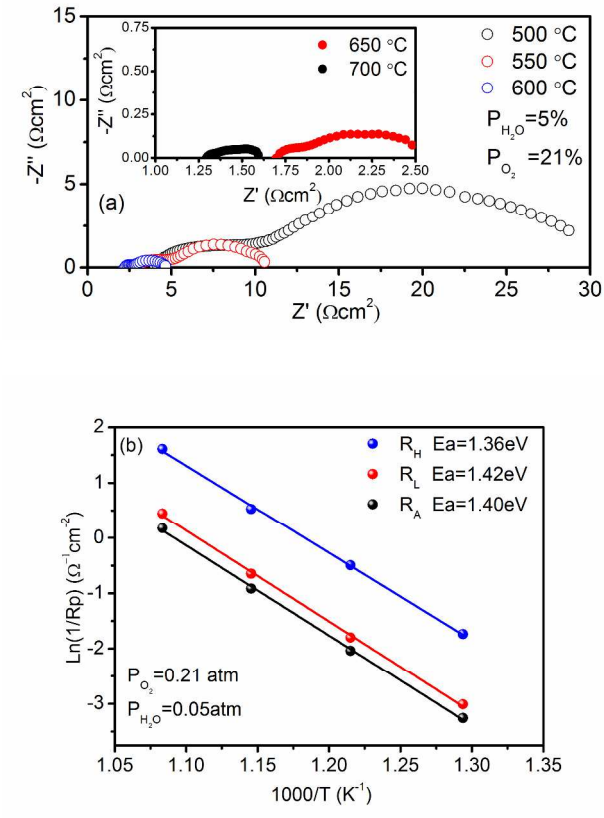

Fig.11 (a) Impedance spectra of the symmetric cell with SFO cathode measured at various temperatures; and (b) the Arrhenius plots of RH,R_L and the total interfacial polarization resistance (Rp).

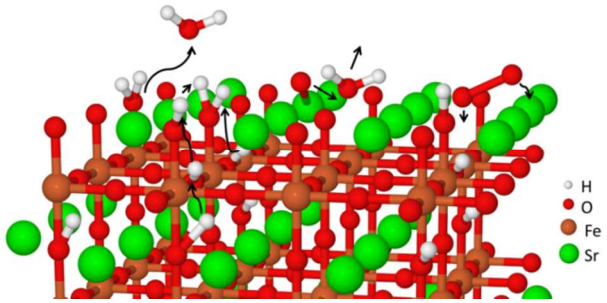

Fig.12. The schematic diagram of the reaction model over the $Sr_3Fe_2O_{7-\delta}$cathode

